Supplementary Information (SI) for ChemComm.

Supporting Information

Revealing Platinum Single-Atom Anchoring Mechanism through Sequential Surface Engineering in $Mo_2TiC_2T_x$ MXene

Bo-Heng Huang [a], Wen-Hsuan Liao[c], Shih-Wen Tseng[d], and I-Wen Peter Chen[a,b,*]

a. Department of Chemistry, National Cheng Kung University No. 1, University Road, East District, Tainan 701, Taiwan. E-mail: iwchen1978@gs.ncku.edu.tw

b. Interdisciplinary Research Center on Material and Medicinal Chemistry, National Cheng Kung University.

c. Department of Earth Sciences, National Cheng Kung University, Tainan, Taiwan

d. Core Facility Center, National Cheng Kung University, Tainan 701, Taiwan

Experimental Section

Synthesis of $Mo_2TiC_2T_x$

To synthesize $Mo_2TiC_2T_x$, 5.0 mL of 98% sulfuric acid (H_2SO_4) and 5.0 mL of 85% phosphoric acid (H_3PO_4) were mixed with 10.0 mL of deionized (DI) water in a Teflon cup. After homogeneous mixing, 1.50 g of ammonium tetrafluoroborate (NH_4BF_4) was added to the acidic solution and stirred until fully dissolved. Subsequently, 0.50 g of $Mo_2TiC_2T_x$ MAX phase powder was dispersed into the etching solution and stirred for 30 minutes to ensure uniform dispersion. The sealed Teflon container was then transferred to a stainless-steel autoclave and subjected to hydrothermal treatment at 180 °C for 24 hours. Upon completion of the reaction, the resulting mixture was centrifuged at 10,000 rpm for 10 minutes. The supernatant was discarded, and the precipitate was repeatedly washed with DI water until the pH of the supernatant approached neutrality. The cleaned solid was then further rinsed and dried in an oven at 55 ℃.

Preparation of electrodes

The catalyst slurry was prepared using a fixed volume ratio of Nafion solution (5 wt%), ethanol (98%), and DI water of 1:10:10 (v/v/v), with all components measured in microliters (µL). Ethanol and DI water were first added to a clean sample vial, followed by the addition of Nafion solution. The mixture was stirred until a homogeneous solvent system was obtained. Subsequently, 10 mg of $Mo_2TiC_2T_x$ powder was introduced and thoroughly mixed to form a uniform slurry. For electrode fabrication, 10 µL of the catalyst slurry was drop-cast onto a carbon paper substrate, producing a coated area of 5 mm × 10 mm. The coated carbon paper was then dried in an oven at 55 ℃ to ensure complete solvent evaporation and firm adhesion of the catalyst layer.

Synthesis of Pt@$Mo_2TiC_2T_x$ (P03-P07)

Electrochemical reduction was performed using a conventional three-electrode configuration in 1.0 M H_2SO_4 electrolyte, with $Mo_2TiC_2T_x$ deposited on carbon paper as the working electrode, a Pt foil as the counter electrode, and an Ag/AgCl electrode as the reference. Cyclic voltammetry (CV) was carried out for 1000 cycles under various potential windows, with all scans initiated from 0 V vs. RHE. The resulting samples were denoted as P0X, where X refers to the terminal negative potential of the CV scan. For example, P07 indicates a sample subjected to potential cycling between 0 and –0.7 V vs. RHE. This one-step synthesis was designed to investigate the electrochemical reduction occurrence on $Mo_2TiC_2T_x$ surface and subsequent single-atom incorporation.

Synthesis of $V_{Mo}/Mo_2TiC_2T_x$ (C03-C07)

Electrochemical reduction was conducted in a standard three-electrode configuration using 1.0 M H_2SO_4 as the electrolyte, with $Mo_2TiC_2T_x$-coated carbon paper as the working electrode, a graphite rod as the counter electrode, and an Ag/AgCl electrode as the reference. CV was performed for 1000 cycles under various potential windows, while maintaining the initial potential at 0 V vs. RHE. The resulting samples were labeled as C0X, where X denotes the terminal potential applied during the CV scan. For instance, C03 represents a sample electrochemically treated within a fix potential window from 0 to -0.3 V vs. RHE. This systematic potential modulation was designed to explore the effects of simultaneously engineering Mo vacancies and surface functional groups in $Mo_2TiC_2T_x$.

Synthesis of Pt@low-V_{Mo}/$Mo_2TiC_2T_x$ and Pt@high-V_{Mo}/$Mo_2TiC_2T_x$

To assess the influence of V_{Mo} density on Pt anchoring, electroreduction was performed via cyclic voltammetry (CV) in a standard three-electrode setup. C03 or C07 was used as the working electrode, with a graphite rod as the counter electrode and Ag/AgCl as the reference electrode. The electrolyte contained Pt ions sourced from the Pt-containing solution recycled from the P09 synthesis to ensure a consistent Pt source. Both C03 and C07 samples underwent 1000 CV cycles under identical mild reduction conditions (0 to –0.3 V vs. RHE). This procedure enabled a direct comparison of Pt incorporation between the two samples. The resulting materials are denoted as Pt@low-V_{Mo}/$Mo_2TiC_2T_x$ (from C03) and Pt@high-V_{Mo}/$Mo_2TiC_2T_x$ (from C07).

Characterizations

The structural properties of samples were obtained by X-ray diffraction (XRD, Bruker, D8 Advance ECO) with Cu Kα radiation (λ= 1.5418 Å). Analytical field emission scanning electron microscope (AFE-SEM, Zeiss, Auriga) and ultrahigh resolution transmission electron microscope (UHR-TEM, JOEL, JEM-2100F+Cs Corrector STEM) which equipped with energy dispersive spectrometer (EDS) were used to observe the morphology and surface properties. The surface bonding was measured by Raman spectroscopy (HORIBA, iHR550) with a laser source wavelength of 532 nm, and X-ray photoelectron spectroscopy (XPS, Thermo Scientific K-Alpha system) with Al Kα X-ray source. Gold (Au) was employed as an internal standard because of its well-characterized and stable photoemission peak, which enables precise spectral alignment. To calibrate the X-ray photoelectron spectroscopy (XPS) data, the binding energy of the Au $4f_{7/2}$ core level was set to 84.0 eV, serving as a reliable reference point. Vacancy concentrations were analyzed via electron paramagnetic resonance (EPR, Bruker EMX-plus system). Elemental compositions were determined by inductively coupled plasma mass spectrometry (ICP-MS, Thermo ELEMENT XR). All the electrochemical tests were measured with multifunctional electrochemical workstation (CH Instruments, CHI7279E) with a three-electrode system consisting of carbon rod counter electrode, working electrode, and Ag/AgCl reference electrode. Photoluminescence phenomenon of material was inspected by fluorescence spectroscopy (PL, HITACHI High-Tech, F 7000) with 150 W Xenon lamp.

Electrochemical test

All electrochemical measurements were conducted using a CHI7279E electrochemical workstation (CH Instruments). A conventional three-electrode system was adopted, in which the as-prepared catalyst served as the working electrode, a graphite rod/Pt foil acted as the counter electrode, and an Ag/AgCl electrode was employed as the reference. The electrolyte solution consisted of 1.0 M H_2SO_4. All potentials were converted to the reversible hydrogen electrode (RHE) scale using the equation:

$$E_{RHE} = E_{Ag/AgCl} + 0.197\ V + 0.059 \times pH$$

Cyclic voltammetry (CV) and linear sweep voltammetry (LSV) measurements were conducted at a scan rate of 1 mV/s, with 85% iR compensation applied. The electrochemical double-layer capacitance (C_{dl}) was evaluated in a non-faradaic region. An estimation of the electrochemically active surface area (ECSA) was carried out to assess the accessible catalytic interface, and the C_{dl} value of the catalyst was divided by the specific capacitance (C_s). The C_s in 1 M H_2SO_4 was taken as 0.035 mF/cm^2.[1-4]

$$ECSA = \frac{C_{dl}}{C_s}$$

Electrochemical impedance spectroscopy (EIS) was conducted across a frequency range of 10^{-2} to 10^6 Hz, with a potential applied at 10 mA/cm^2 to investigate the performance in hydrogen and oxygen evolution reactions.[5, 6]

Calculate TOF value to quantitatively demonstrate the atomic-level catalytic efficiency under ultralow Pt loading:[7]

$$TOF = \frac{mol\ of\ H_2\ generated\ per\ second}{mol\ of\ surface\ Pt\ atoms} = \frac{I}{2F \times n_{Pt}}$$

H_2

$$= j\frac{mA}{cm^2} \times \frac{1\ Cs^{-1}}{1000\ mA} \times \frac{1\ mol\ e^-}{96485.3\ C} \times \frac{1\ mol\ H_2}{1\ mol\ e^-} \times \frac{6.022 \times 10^{23}\ H_2}{1\ mol\ H_2} = 3.12 \times 10^{1}$$

cm^{-2}

$$TOF = \frac{3.12 \times 10^{15} \times |j|}{Pt\ active\ site}$$

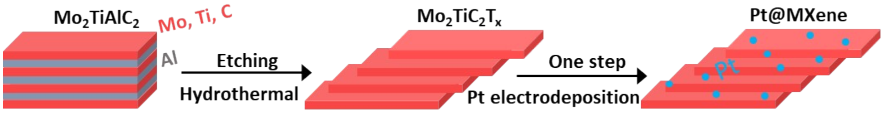

Fig. S1 Schematic illustration of the mild etching strategy and following single-step electrochemical reduction. Etchant: Sulfuric acid (H_2SO_4), phosphoric acid (H_3PO_4), deionized (DI) water and ammonium tetrafluoroborate (NH_4BF_4).

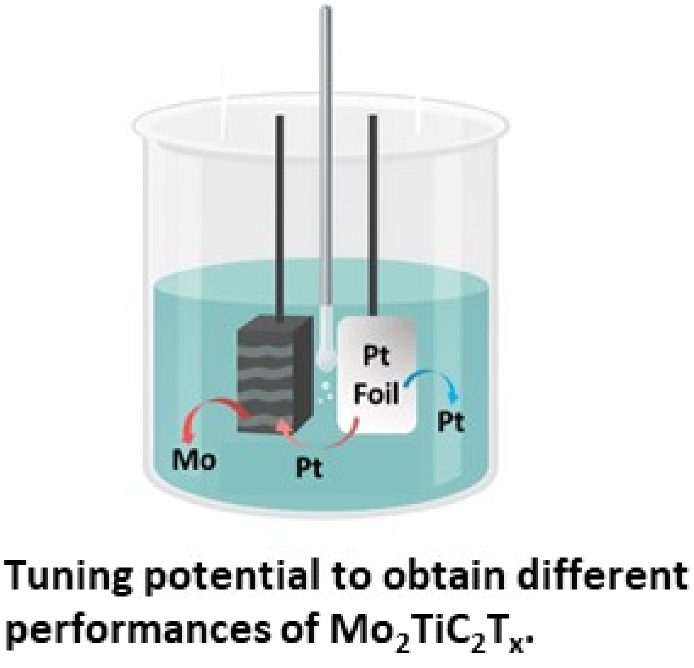

Fig. S2 Schematic of preparation for Pt@$Mo_2TiC_2T_x$ by electroreduction.

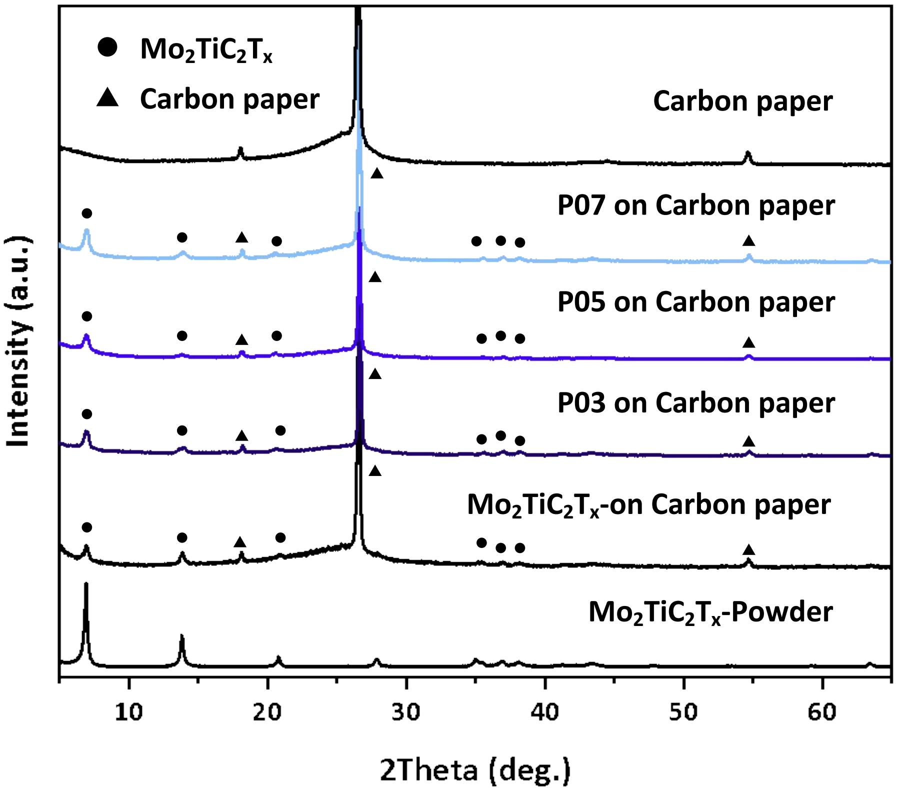

Fig. S3 XRD patterns after electrochemical treatments at different potentials showing no structural distortion.

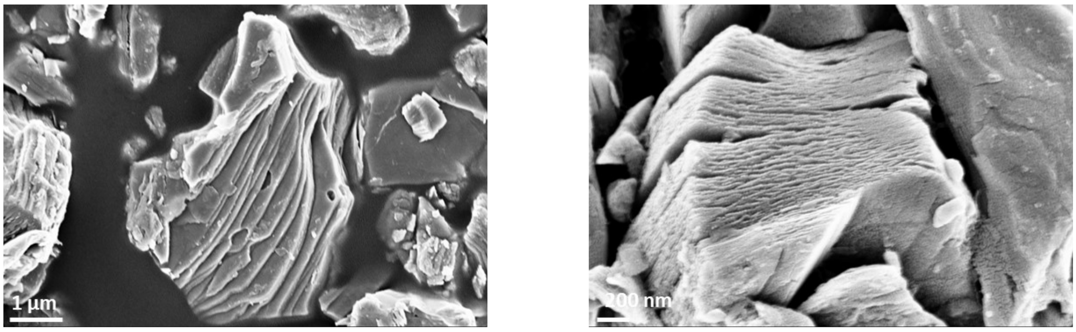

Fig. S4 SEM images of the synthesized $Mo_2TiC_2T_x$ open layered morphology. Low-resolution (left) and high-resolution (right).

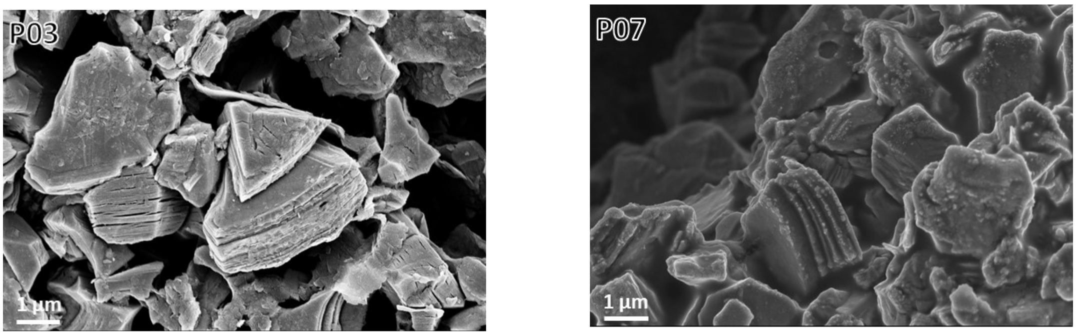

Fig. S5 SEM images of P03 (left) and P07 (right) that the characteristic open layered morphology remained intact across all samples.

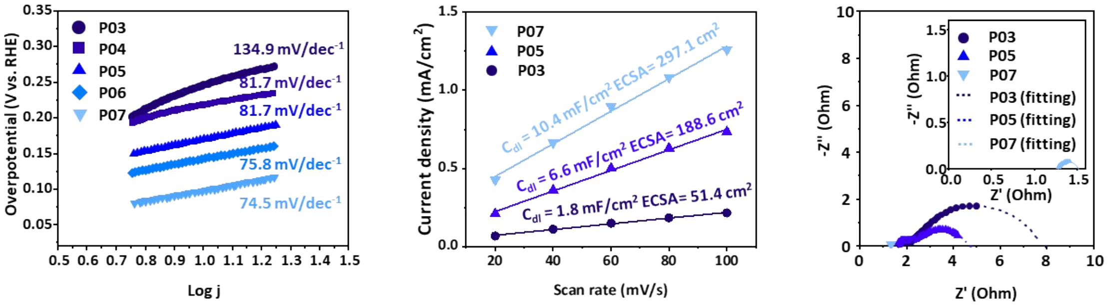

Fig. S6 Tafel slopes, ECSA, and EIS of P03, P04, P05, P06 and P07 samples (from left to right).

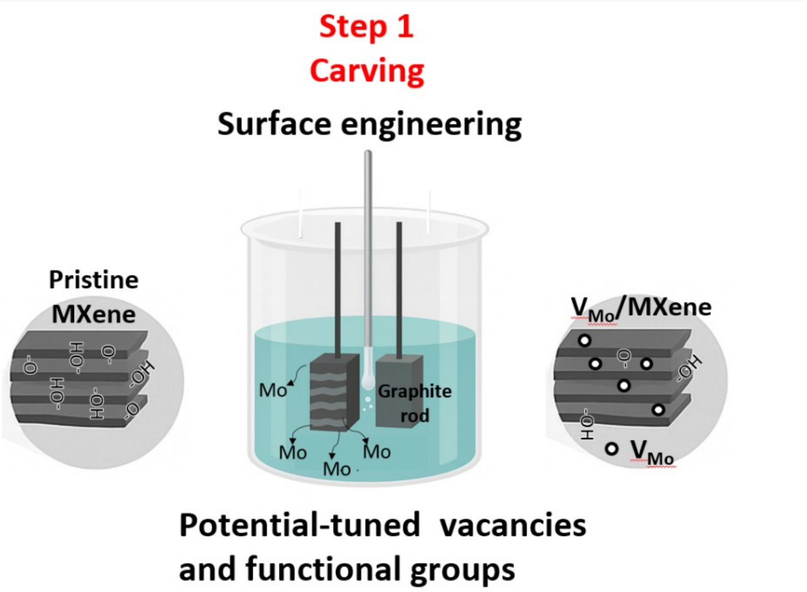

Fig. S7 Schematic of preparation for “carving” treatments at different potentials. 1.0 M H_2SO_4 as the electrolyte, with $Mo_2TiC_2T_x$-coated carbon paper as the working electrode, a graphite rod as the counter electrode, and an Ag/AgCl electrode as the reference. The carving treatment modulates vacancies and functional groups in the MXene.

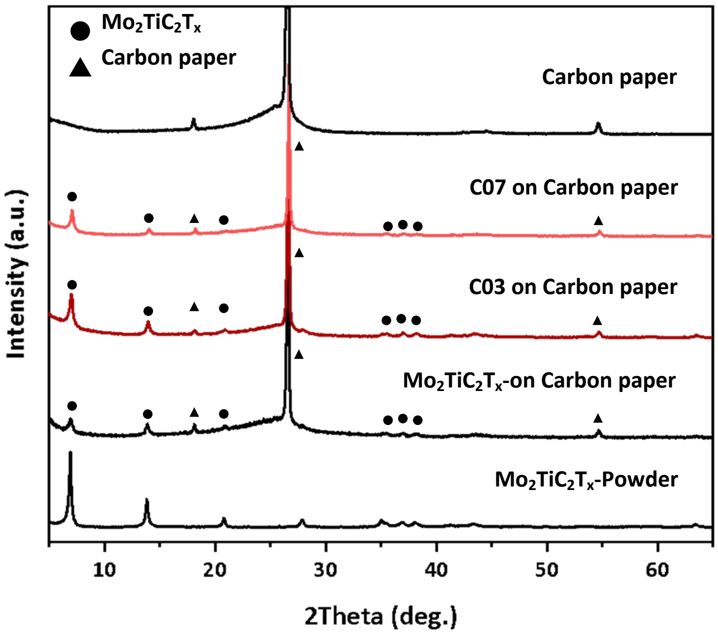

Fig. S8 XRD of $Mo_2TiC_2T_x$, C03 and C07 showing identical structural patterns.

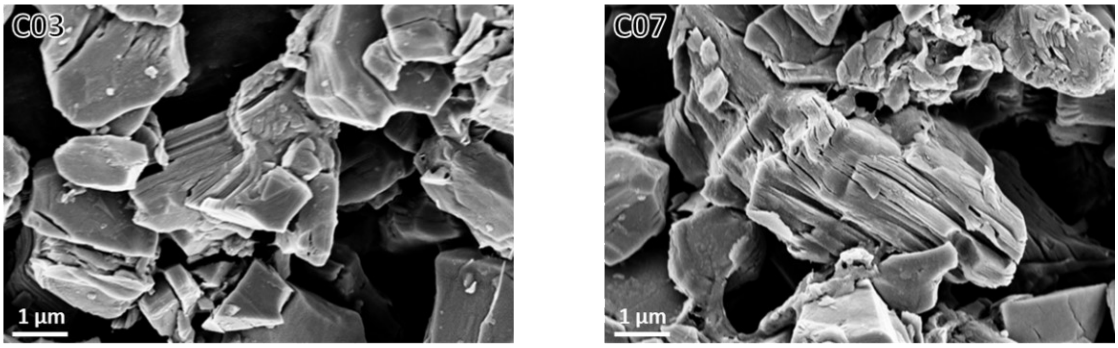

Fig. S9 SEM images of C03 (left) and C07 (right) confirmed that the characteristic open layered morphology remained.

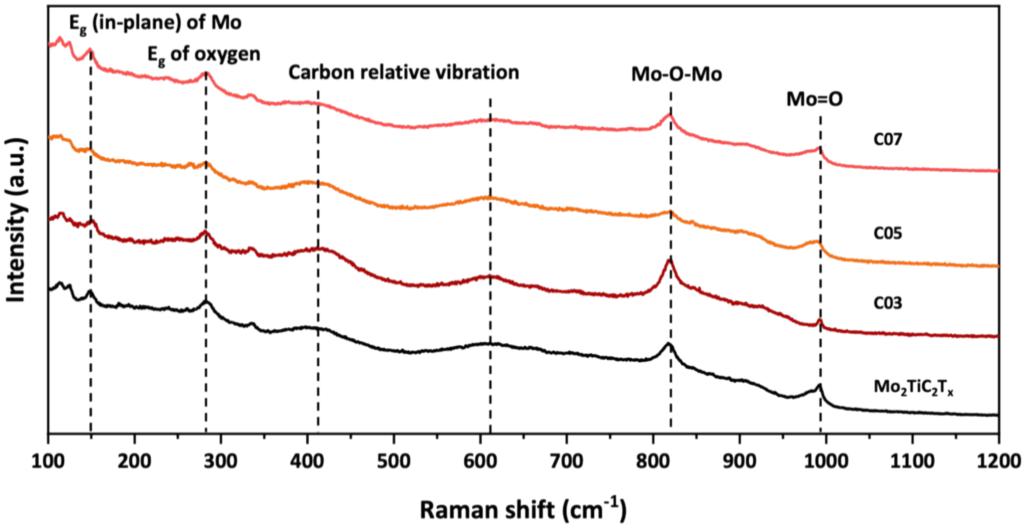

Fig. S10 Raman spectra of $Mo_2TiC_2T_x$, C03, C05 and C07. The Raman mode at 148 cm^{-1} is assigned to the E_g vibrations involving both Mo and Ti atoms, while the feature near 277 cm^{-1} corresponds to the E_g vibration of oxygen, indicating the presence of Mo–O bonding in the MXene. The bands observed at approximately 401 and 603 cm^{-1} are predominantly attributed to vibrations of carbon atoms within the MXene lattice. In addition, Raman features at 818 and 985 cm^{-1} are associated with oxygen-containing surface terminations. When normalized to the E_g vibration of Mo, the relative intensities of all oxygen-related Raman modes systematically decrease with increasing applied potential, indicating a progressive depletion of oxygen-containing surface functional groups at higher potentials.[8-10]

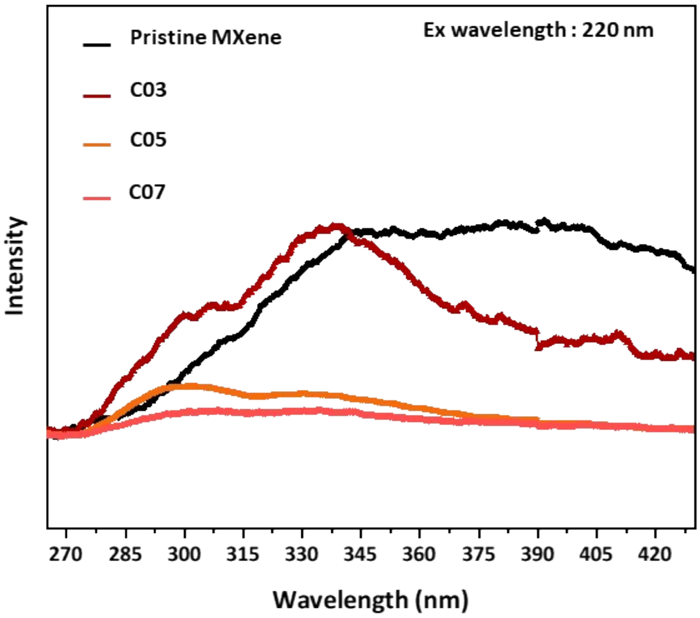

Fig. S11 Photoluminescence (PL) spectra of $Mo_2TiC_2T_x$, C03, C05 and C07. The gradual suppression of the broad emission band reveals an enhancement in trap-state density, which accelerates nonradiative recombination and leads to the observed PL quenching.

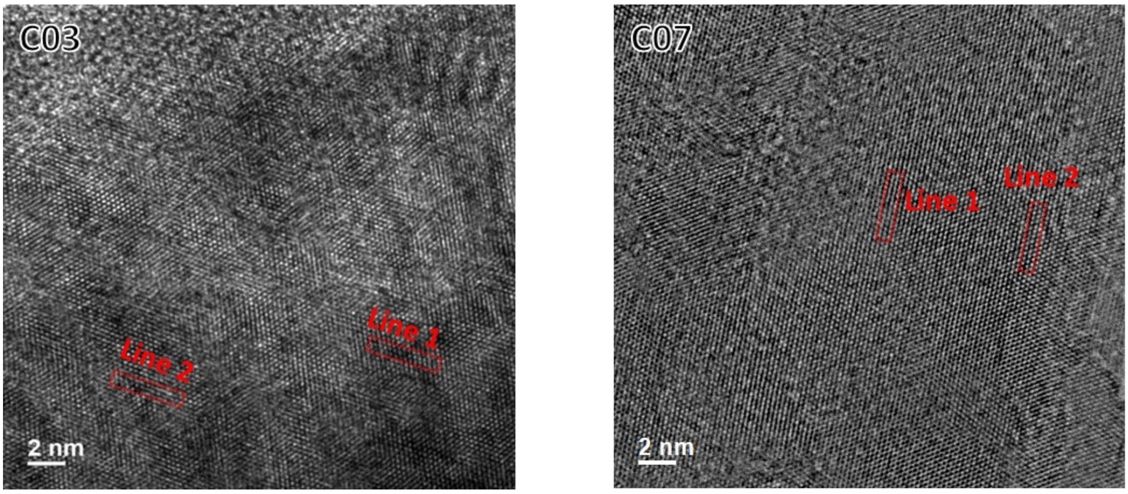

Fig. S12 High-resolution transmission electron microscopy (HR-TEM) of C03 (left) and C07 (right).

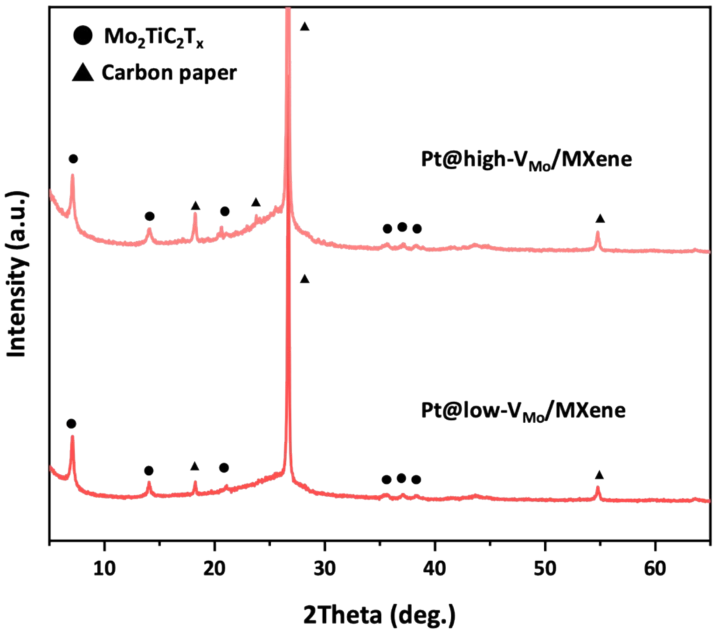

Fig. S13 XRD of Pt@low-V_{Mo}/$Mo_2TiC_2T_x$ and Pt@high-V_{Mo}/$Mo_2TiC_2T_x$ showing identical structural patterns.

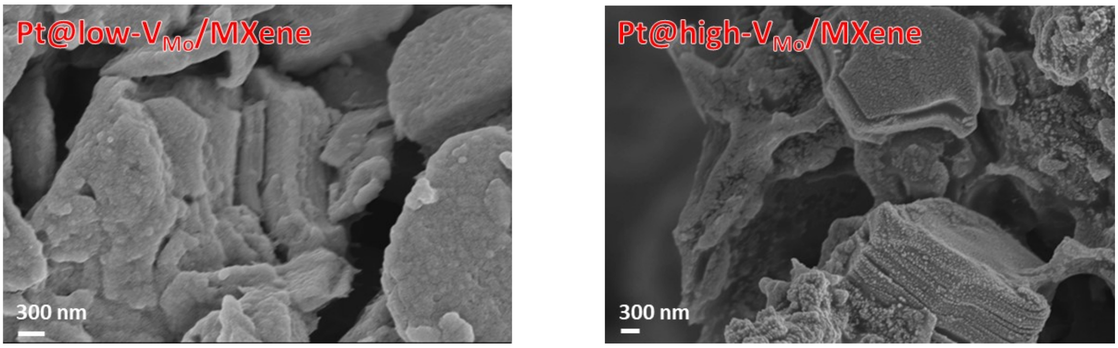

Fig. S14 SEM images of Pt@low-V$_{Mo}$/MXene (left) and Pt@high-V$_{Mo}$/MXene (right) confirmed that the characteristic layered morphology remained.

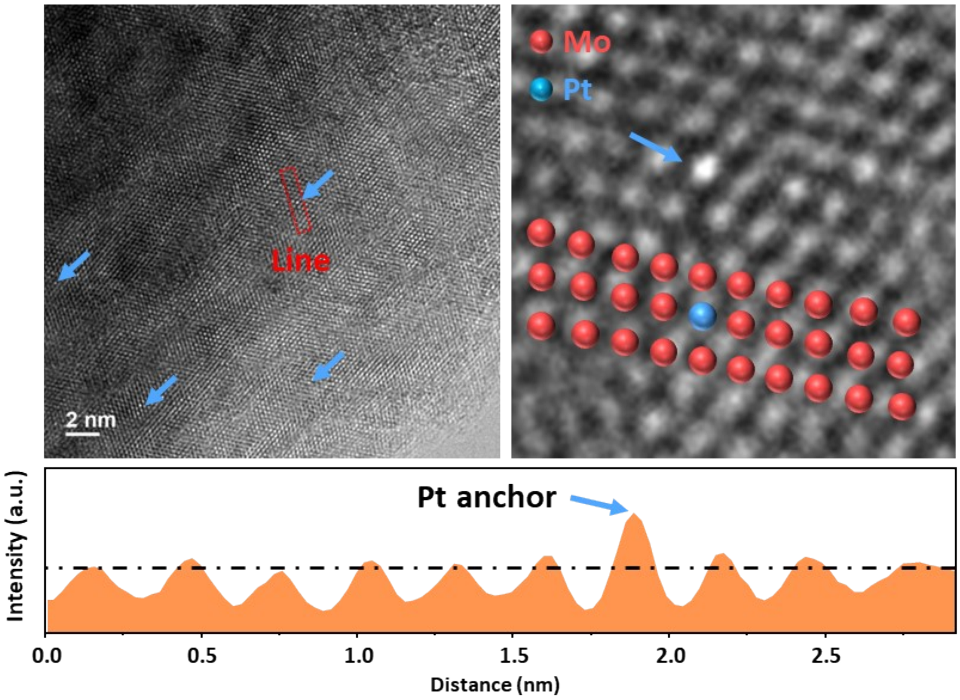

Fig. S15 Atomic-resolution transmission electron microscopy (TEM) of Pt@low-V_{Mo}/$Mo_2TiC_2T_x$, suggesting inefficient anchoring due to the scarcity of suitable binding sites.

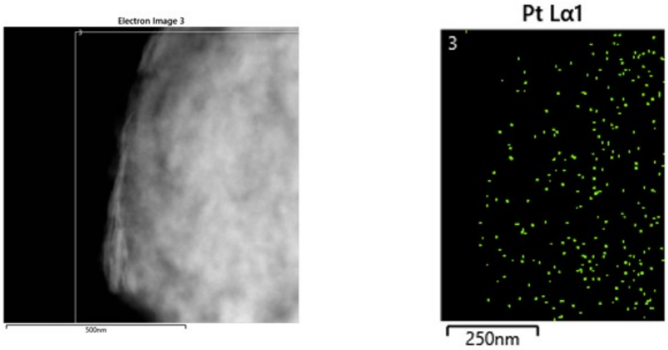

Fig. S16 High-resolution EDS elemental mapping Pt@high-V_{Mo}/$Mo_2TiC_2T_x$, suggesting the global dispersion of Pt.

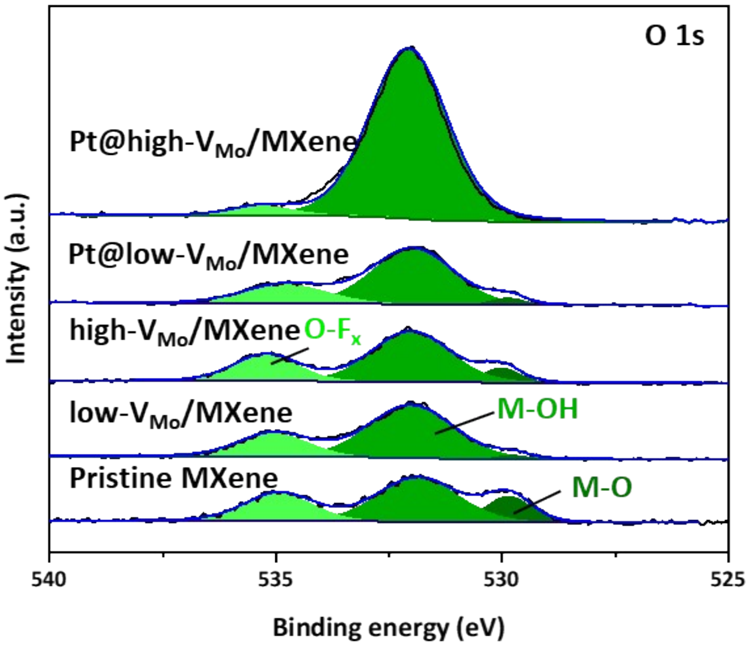

Fig. S17 XPS spectra of O 1s of different treated samples which showed a decline in the intensity of the metal–oxygen bond component after Pt anchoring.

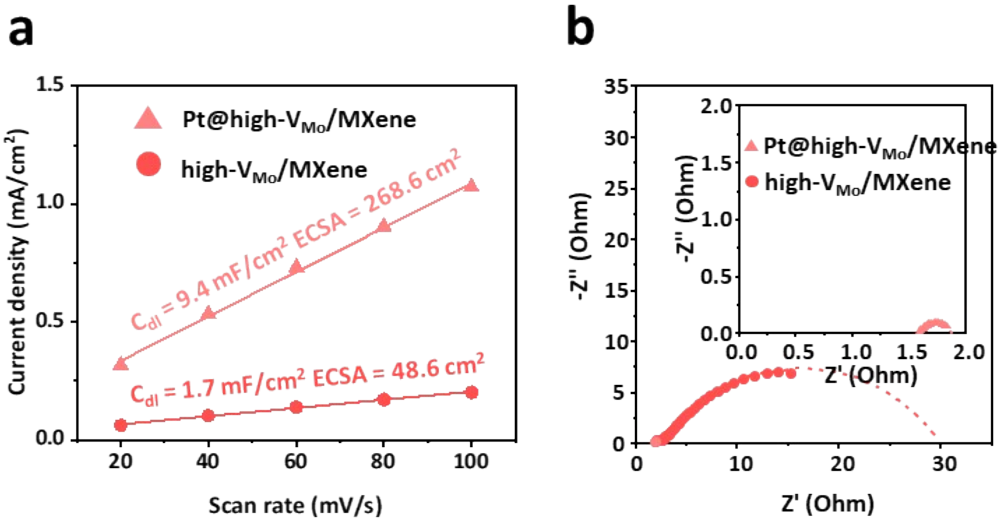

Fig. S18 a) ECSA and b) EIS of samples before and after patching stage.

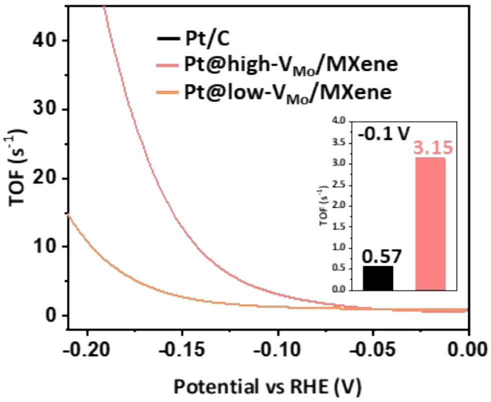

Fig. S19 TOF plots of Pt@low-V_{Mo}/$Mo_2TiC_2T_x$ and Pt@high-V_{Mo}/$Mo_2TiC_2T_x$. The Pt@high-V_{Mo}/MXene catalyst exhibits a TOF of 3.15 H_2·s^{-1}·Pt atom^{-1} at 100 mV vs. RHE, which is substantially higher than that of commercial Pt/C reported in the literature under comparable conditions (~0.57 H_2·s^{-1}·Pt atom^{-1}).[11]

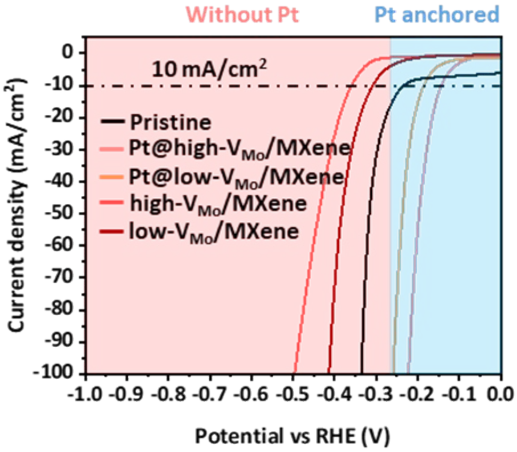

Fig. S20 LSV curves of all characteristic samples.

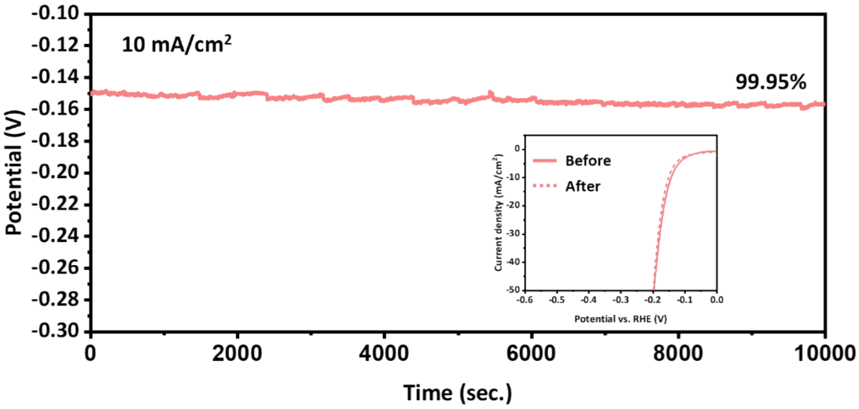

Fig. S21 Long-term HER catalytic stability tests. Chronopotentiometric (CP) curve of Pt@high-V_{Mo}/$Mo_2TiC_2T_x$ at a constant current density of 10 mA cm^{-2} for 10,000 s and LSV curves recorded before and after the 10,000 s stability test.

Table S1 Integral area of Raman peak and relative oxygen-related ratio to Mo.

Mode		Raman shift	Pristine	C03	C05	C07
E_g in-plane vibration of Mo atom	(1)	148 cm^{-1}	89188.6	42809.8	61153.8	78686.7
E_g vibration of the O atoms	(2)	277 cm^{-1}	161118	73645.7	103863	124551
Oxygen functionalization	(3)	818 cm^{-1}	98238.2	48179.4	62122.9	73070.8
	(4)	985 cm^{-1}	37293.6	16992.4	27825.2	31540
Relative oxygen-related ratio to Mo	{[(2)+(3)+(4)]/(1)}		3.3261	3.2426	3.1692	2.9123

Reference

1 J. D. Benck, Z. Chen, L. Y. Kuritzky, A. J. Forman and T. F. Jaramillo, *ACS Catal.*, 2012, **2**, 1916–1923.

2 S. Trasatti and O. A. Petrii, *Pure Appl. Chem.*, 1991, **63**, 711–734.

3 C. C. L. McCrory, S. Jung, J. C. Peters and T. F. Jaramillo, *J. Am. Chem. Soc.*, 2013, **135**, 16977–16987.

4 X. Zhang, J. Chacón-Borrero, R. He, J. Gázquez, M. Torras, A. Cabot, A. Roig and P. Guardia, *J. Mater. Chem. A*, 2025, **13**, 7721–7730.

5 V. M.-W. Huang, V. Vivier, M. E. Orazem, N. Pébère and B. Tribollet, *J. Electrochem. Soc.*, 2007, **154**, C99.

6 G. J. Brug, A. L. G. van den Eeden, M. Sluyters-Rehbach and J. H. Sluyters, *J. Electroanal. Chem. Interfacial Electrochem.*, 1984, **176**, 275–295.

7 International Union of Pure and Applied Chemistry (IUPAC), 5.0.0 edn., 2025, DOI: doi:10.1351/goldbook.T06534.

8 G. Li, B. Zhou, P. Wang, M. He, Z. Fang, X. Yuan, W. Wang, X. Sun and Z. Li, *Catalysts*, 2022, **12**, 850.

9 M. W. Hakim, I. Ali, S. Fatima, H. Li, S. H. M. Jafri and S. Rizwan, *ACS Omega*, 2024, **9**, 8763–8772.

10 A. Sarycheva and Y. Gogotsi, *Chem. Mater.*, 2020, **32**, 3480–3488.

11 F.-Y. Yu, Z.-L. Lang, L.-Y. Yin, K. Feng, Y.-J. Xia, H.-Q. Tan, H.-T. Zhu, J. Zhong, Z.-H. Kang and Y.-G. Li, *Nat. Commun.*, 2020, **11**, 490.